JOURNAL OF MATERIALS SCIENCE **39** (2004) 2121–2130

Dual scale non-linear stress analysis of a fibrous metal matrix composite

J. H. YOU*, O. POZNANSKY
Max-Planck-Institut für Plasmaphysik, Euratom Association, Boltzmannstr. 2, D-85748 Garching, Germany
E-mail: jeong-ha.you@ipp.mpg.de

Precise estimation of local stress profiles in individual phases of a fiber reinforced metal matrix composite is a crucial concern for design of composites. Stress profiles are significantly affected by plastic relaxation of soft matrix. In this work, an analytical model was developed to compute local stress profiles in individual phases of fibrous metal matrix composites. To this end, embedded cell cylindrical composite model was applied in which a layered concentric cylinder consisting of a fiber-, matrix- and homogenized composite layers was used. Mean field micromechanics was integrated into the conventional elasticity solution process so that micro-macro dual scale analysis could be performed. The algorithm was formulated in an iterative incremental structure which was able to perform plastic analysis. This also allows temperature dependence of flow stress to be considered. Taking copper-SiC system as a reference composite, stress profiles were obtained for mechanical and thermal loading cases. For comparison, independent finite element analyses were carried out for two different unit cell models. Excellent agreement between analytical and numerical solutions was found for the mechanical loading case even for plastic range. In the case of thermal loading, however, plastic solutions revealed notable difference in quantity, especially for the axial stress component.

1. Introduction

Fiber reinforced metal matrix composites (FRMMCs) are being considered as a candidate material group for several advanced structural applications, since they possess significantly extended creep resistance, strength and dimensional stability [1]. The ultimate load carrying capacity of the composites will be limited by progressive plastic flow of matrix or by clustering of fiber fracture [2, 3].

Accurate determination of stress states being generated in individual phases of a FRMMC is a crucial concern to understand the mechanisms of microstructural damage modes. For instance, plastic ratcheting and void formation in matrix are attributed to repeated reverse of deviatoric stresses and triaxiality of principal stresses, respectively [4]. On the other hand, interfacial debonding and fiber fracture are ascribed to fracture mechanical stress intensity [3].

In the case of composite with ductile matrix, stress profiles will be significantly affected by plastic relaxation of soft matrix, especially at elevated temperatures. Hence, incorporation of plasticity into mechanics-based damage prediction is mandatory. In the following, we assume that plastic yield to be the most dominant factor of stress relaxation and other inelastic effects to be negligible.

Diffraction techniques using X-ray or neutron beam have been the most commonly applied experimental tools for the measurement of residual stresses generated in a composite material [1]. However, due to low spatial resolution and practical difficulties concerned with *in-situ* measurement during loading, its application fields have been rather limited. This suggests that complementary theoretical evaluation is required for complete assessment of stress states in a FRMMC.

Numerical analysis based on the finite element method would provide us with relatively accurate solution when the used model is realistic enough. In the case of complex loading or irregular fiber array, three dimensional models or the method of representative volume element should be used, which may be quite costly in certain case [1, 5].

Within the framework of analytical studies several approaches have been suggested for elastic fibrous composites in which various elastic models of load transfer were used. Especially, the mechanics models formulated on the basis of the Eshelby transformation tensor or those based on the conventional procedure of elastostatics have formed the main stream [1, 6].

Exact stress solutions were obtained for single-fiber elastic composite systems either with infinite matrix or with bounded matrix. Method of the Eshelby transformation tensor as well as that of the conventional

*Author to whom all correspondence should be addressed.

elasticity were successfully applied [7–10]. It was proved that these two independent analytical approaches produced identical or nearly the same results regardless of loading nature, i.e., for both thermal and mechanical load cases [1, 7].

However, the elastic stress solutions for single-fiber systems combined with infinitely extended matrix are valid only for a composite with extremely small fiber content. To include the constraint effect of neighboring fibers which would become more conspicuous as fiber content increases, the single-fiber model may be modified by replacing the infinite matrix with bounded finite matrix so that the latter system would have the same fiber content as the multi-fiber counterpart under consideration. This modification can be applied to one of the aforesaid analytical methods [1].

But, solutions for a single-fiber system with bounded matrix would not exactly represent the realistic stress profiles occurring in a many-fiber system having the equivalent fiber content. This can be easily understood by noting that the approximation based on the single-fiber system fails near the outer boundary of matrix layer due to free surface effect which would not exist in the interior of a real composite [11]. For correction of this problem, an additional boundary condition has to be imposed onto the matrix surface [12].

In the case of multi-fiber composite systems, micromechanical theories based on the Mori-Tanaka mean field method have drawn increasing attention in the last two decades [13]. These Mori-Tanaka type formulations can provide a closed form solution for an elastic composite having a simple geometry and low fiber content (less than approximately 20 vol%). It was also shown that they could be extended to plastic regime [14]. This allowed overall plastic behavior to be predicted in global scale. However, the mean field solutions are insufficient for precise determination of local stress profiles, since stress components are averaged in each phase volume. Mean field methods have an intrinsic restriction for determination of local stress profiles.

Mikata and Taya developed a modified single-fiber composite model in which a layered concentric cylinder composite was considered [7]. Their system consisted of a fiber, matrix and surrounding effective composite media forming a three layer system (actually, they included an additional layer of fiber coating in their work). In this paper, we term this kind of geometrical model 'embedded cell cylindrical composite model' (ECCC model), where the term 'cell' stands for the domain occupied by fiber and matrix. In their work, the outermost effective layer was assumed to be infinite.

The stress solution was derived from a conventional method of elasticity. To obtain the effective properties of homogenized composite layer, they used the classical rule of mixture (by Voigt or Reuss).

Geometrical analogy can be easily found between the ECCC model and the generalized self-consistent model, an extended version of the classical self-consistent method [15]. It should be noted that the latter used a self-consistent mean field formalism to compute the effective stiffness of whole composite system whereas no micromechanical method was employed in the former model. It was pointed out by Warwick and Clyne that the use of effective properties for composite layer is not rigorous [11]. In addition, this concept is not flexible in its form for the extension to plastic formulation.

The aim of present work is to develop an analytical model with which the constraint effect of surrounding fibers and the effect of plastic flow of matrix can be included in a consistent manner.

To this end, the elastic ECCC model of Mikata and Taya was modified by application of mean field micromechanics which replaced the rule of mixture method. In addition to determination of effective properties of composite layer, dual scale analysis was achieved by the micromechanics technique. Further, incremental computation was performed to include nonlinear nature of matrix yield.

Taking copper-SiC system as a reference FRMMC, stress profiles were calculated for mechanical and thermal loading cases. The results were compared with those of FEM analysis carried out for unit cell models.

2. Model description

The ECCC model to be formulated in this work is based on a concentric multi-layered cylindrical geometry with axial symmetry. In Fig. 1, a three layer system is illustrated schematically. It consists of a fiber, matrix and effective composite layer. In terms of ECCC model the domain occupied with the fiber and the matrix being surrounded by the effective composite layer forms a cell.

Elastic part of the analytical framework of present model is not much different from that of conventional elastic solutions derived for many layer systems subjected to thermo-mechanical loads. In this work, the elastic solution algorithm of Warwick is used, since it

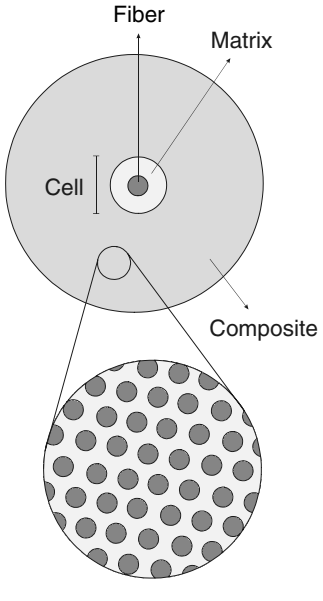

Figure 1 Schematic illustration of ECCC model geometry showing a layered concentric composite cylinder. This cylinder consists of a fiber, matrix and effective composite layer. Micro-macro dual scale analysis is performed in the effective composite layer via mean field micromechanics.

is written for the most general case of arbitrary number of layers [11].

Characteristic feature of present model is that a micromechanical method was integrated into the foregoing elastic solution procedure. Within this hybrid procedure stress analysis could be performed on dual scales (i.e., micro and macro) for the effective composite layer.

This concept is visualized in Fig. 1 using a fictitious microscope. Matrix plasticity was taken into account by means of Euler backward incremental integration scheme. The combination of dual scale analysis with Euler backward incremental integration allowed self-consistent stress analysis.

The applied micromechanical method was based on the work of Pettermann [16]. His algorithm is an elasto-plastic version of the originally elastic Mori-Tanaka type mean field theory formulated by Benveniste [17].

3. Computational procedure

Structure of the computational procedure is plotted in Fig. 2 in a simplified form. This flowchart indicates the linkage of the three separate modeling units, i.e., the elastic ECCC module, micromechanics module and the plasticity module, respectively. In Fig. 3, a more detailed description of the procedure is presented. The mathematical steps explained in Appendices A and B are systematically illustrated. The thick arrows indicate the main stream of the computation while the thin one stands for data exchange or substitution of results.

First, all necessary data (material properties, geometry) are input via separate data files. Temperature dependence of matrix flow stress can be also considered. With input of specified load increment (either mechanical or thermal) and of prescribed total load, the first incremental step of computation is triggered.

In the first module, elastic stress profiles are determined for a given composite system by means of Warwick's algorithm. Mathematical steps of this algorithm are written in Appendix A. In this first stage the Eshelby's micromechanics is already at work producing the effective thermo-elastic composite properties which are used as input data for elastic ECCC model.

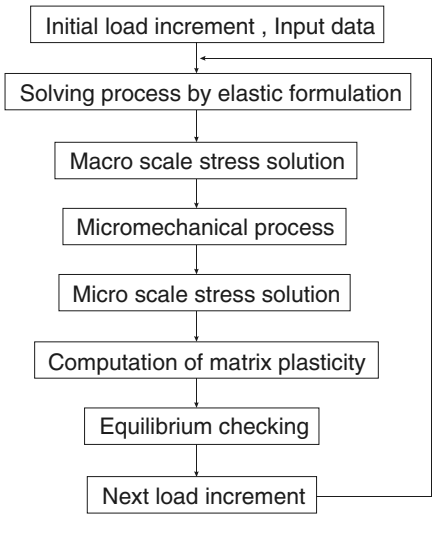

Figure 2 Conceptual flowchart showing the structure of computational procedure. Three separate modeling units, that is, elastic ECCC module, micromechanics module and plasticity module are indicated.

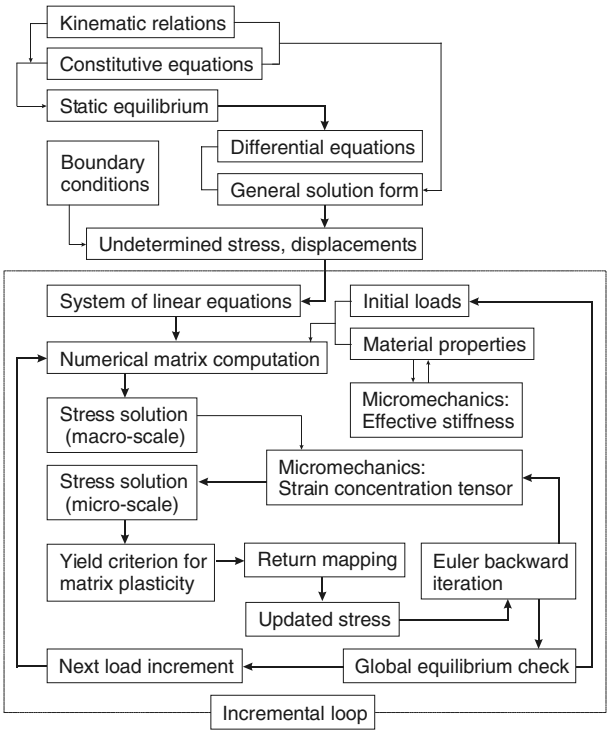

Figure 3 Detailed description of the algorithm. Thick arrows indicate main stream of the computation while thin one stands for data exchange or substitution of results.

In the second module, the local mean field stress in the matrix of the homogenized composite layer is calculated from the foregoing global elastic solution using the stress- or strain concentration tensor of Benveniste's micromechanics model.

In the last module, yield criterion is checked for the current total stress state in the matrix of the composite layer as well as in the matrix of the cell. The stress level in both regions should be identical. Here the elastic stress increment is considered as elastic predictor in terms of radial return mapping method which is a kind of Euler backward incremental integration method [18].

When the yield criterion is satisfied (that is, when the predictor vector ends outside of matrix yield surface), stress updating is performed according to the radial return mapping algorithm. When updating of the matrix stress state is completed, all other micromechanical state quantities have to be updated too so that these quantities have proper instantaneous values after plastic relaxation of matrix.

This step must be carried out by an internal iteration process due to characteristic Euler backward response of macroscopic composite strain to updating of microscopic matrix strain. Global force equilibrium should be checked again after stress updating. If existing, offset stress should be reduced by modifying the final matrix stress vector on the yield surface in order that the force equilibrium is achieved within a given tolerance.

The procedure is repeated in subsequent load increments until the prescribed total load is reached. The total matrix stress is determined by superposition of the elastic stress increment (predictor) obtained from

current elastic ECCC analysis onto the instantaneous stress state delivered from the previous increment.

After onset of plastic flow, the Eshelby tensor should be estimated numerically due to the matrix anisotropy induced by flow. Here, the Gauss quadrature algorithm by Lagoudas and Gavazzi was used [19]. Fundamentals of the Pettermann's Incremental mean field formulation is explained in Appendix B.

4. Test calculation

To verify the performance of present model, two different test calculations were carried out. The loading conditions assumed for the test calculations were as follows:

(1) a mechanical loading in axial direction with far field applied stress of 100 MPa,
(2) a thermal loading with uniform temperature drop of 100°C.

For comparison, independent finite element analyses (FEA) were conducted. For FEA, unit cell models were applied, since their geometry is distinct from that of the ECCC model.

As reference material, a copper matrix composite reinforced with 20 vol% SiC long fibers was taken. It was assumed that the SiC fiber (radius: 70 μm) was coated by thin graphite layer (1 μm thick) forming a perfect interfacial bonding to matrix. For brevity, this graphite coating was not considered in FEA. Cross-sectional geometry of the reference composite is shown in Fig. 4. It should be noted that the SiC fiber contains a tungsten core (radius: 15 μm) at its center. The material properties are listed in Table I. Outer radius of the composite was varied from 500 to 3000 μm to estimate the effect of composite layer thickness on stress results. The specified load increment was 1 MPa for both mechanical and thermal (conversed from temperature increment) load cases.

In FEA, two kinds of unit cell models were used: hexagonal and square array. Geometry of the cell cross sections is shown in Fig. 5. Three dimensional models meshed with second order elements were used. Symmetry boundary conditions were imposed assuming infinite extension of the composite.

It should be mentioned that FEA for the present ECCC model geometry was also carried out using commercial code ANSYS to check the numerical performance of the algorithm itself. No meaningful error was found from this cross checking test.

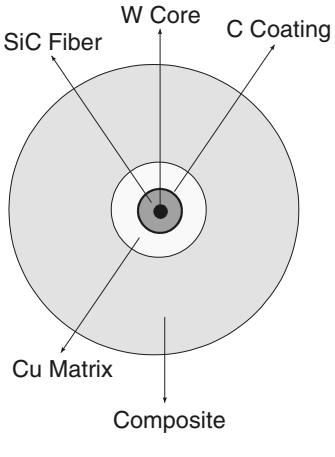

Figure 4 Cross-sectional geometry of the reference composite used for the ECCC test calculation. This reference composite consisted of copper matrix and 20 vol% SiC long fiber reinforcement. Dimensions were as follows: tungsten core (radius: 15 μm), SiC fiber (radius: 70 μm), graphite layer (1 μm thick), effective composite (radius: 500–3000 μm).

TABLE I Properties of matrix and fiber materials at room temperature [1, 20]

	W fiber	SiC fiber	Graphite	Copper
Young's modulus (GPa)	405	450	400	130
Poisson's ratio	0.29	0.17	0.15	0.34
Coefficient of linear thermal expansion (10^{-6}/K)	4.5	5.7	10	16.7
Yield stress (MPa)	1050			44

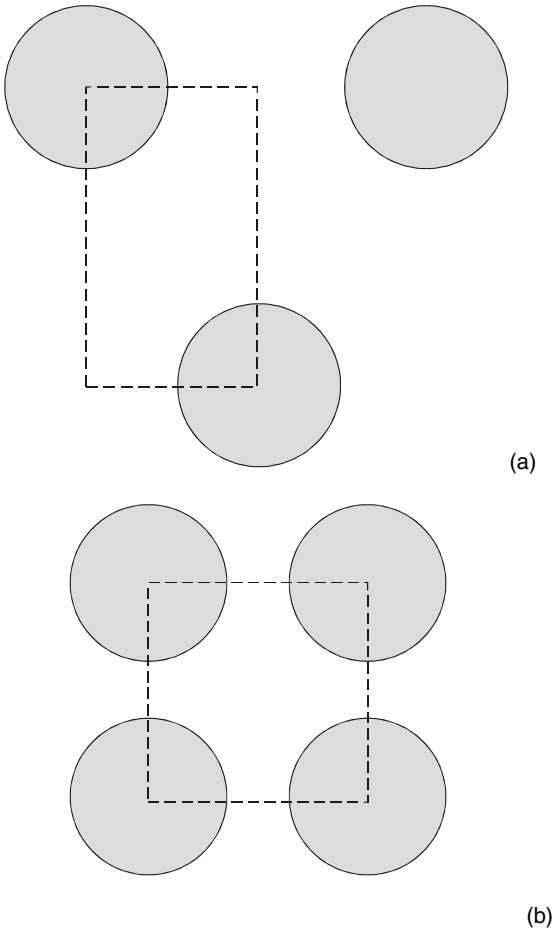

Figure 5 Cross sectional geometry of the two unit cell models used for finite element analysis (FEA) to which three dimensional models with hexagonal and square array were applied.

5. Results and discussion

Predicted mechanical and thermal stress profiles for plastic as well as elastic cases are presented in Figs 6–9, respectively. Analytical solutions from the ECCC model are compared with numerical solutions from the FEA of unit cell models. Results are plotted for three principal stress components along the radial position starting from the symmetry axis of the composite

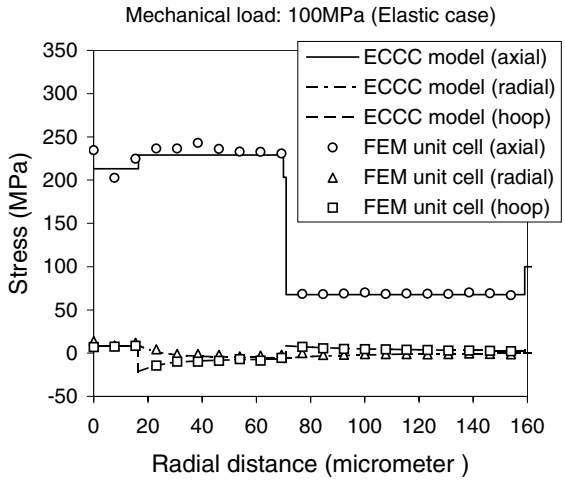

Figure 6 Predicted elastic stress profiles calculated for applied axial stress of 100 MPa. Analytical solutions from the ECCC model are compared with numerical solutions from FEA using unit cell model (hexagonal). Results are presented only for the cell domain.

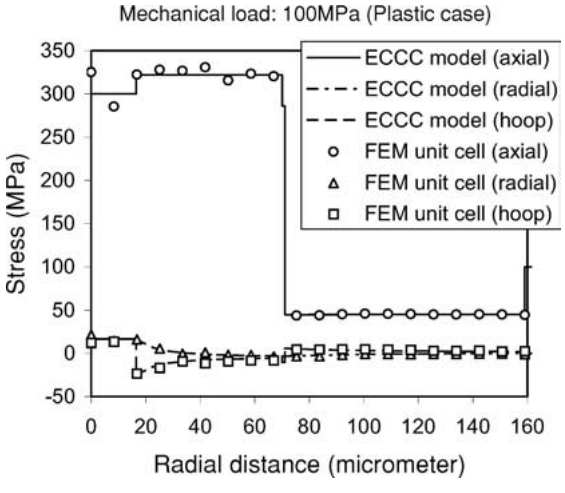

Figure 7 Predicted plastic stress profiles calculated for applied axial stress of 100 MPa.

cylinder up to the cell boundary (i.e., outer boundary of the matrix layer).

Figs 6 and 7 show excellent agreement between analytical and numerical solutions for the mechanical loading even in the plastic case. Distribution of the triaxial stress states after relaxation could be accurately reproduced. The local mean field stresses of matrix and fiber in homogenized composite layer had same values as those of volume averaged stresses of matrix and fiber in the cell, respectively. This indicates the self-consistence of the ECCC model.

In the case of thermal loading, however, such an exact coincidence could not be obtained. While the elastic ECCC solution shows similarity to numerical one (Fig. 8), plastic solution reveals notable difference, especially for the axial stress component (Fig. 9). This may be attributed to severe thermal stress gradient which could cause enhanced numerical errors by averaging operation during mean field homogenization. The tensile hoop stress in the thin graphite coating increased sharply upon plastic flow of matrix. This suggests that crack in the graphite coating would propagate along the fiber axis direction.

It is noticed that the two unit cell models produced nearly identical thermal stress profiles except the fiber-matrix interface region. Actually, no difference in work hardening rate of this composite was observed between the two unit cell models [21]. In principle, change of unit cell geometry can lead to a significant difference in stress level and in global work hardening behavior when fiber volume fraction becomes higher ($f \simeq 0.5$) [22].

Variation of the composite layer thickness t_c had actually no influence on the results in the range $t_c \geq 5R$ (R: fiber radius). This fact provides a guideline how much a tensile test specimen of a FRMMC can be downsized without inducing any deviation of stress state from that of large size one.

6. Summary

In this work, an analytical model was developed to compute local stress profiles in individual phases of fiber reinforced metal matrix composites. To this end, embedded cell cylindrical composite model was applied in which a layered concentric cylinder consisting of a fiber, matrix and effective composite layers was used.

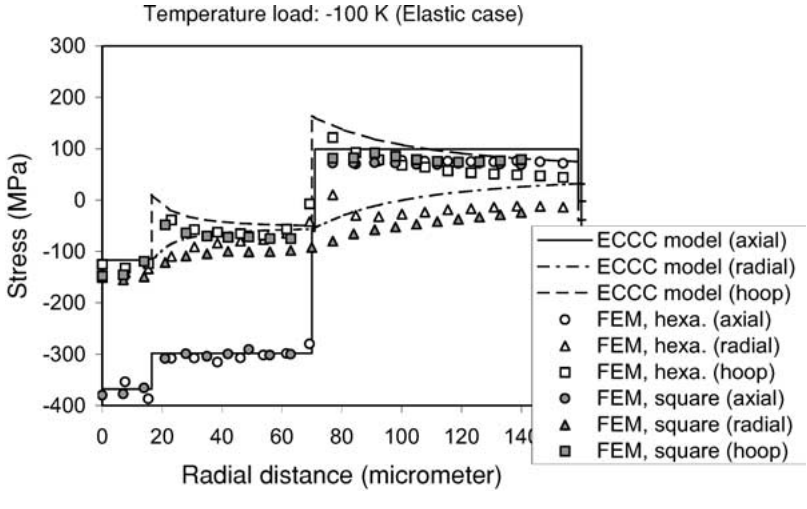

Figure 8 Predicted elastic thermal stress profiles calculated for temperature decrease of 100°C. Analytical solutions from the ECCC model are compared with numerical solutions from FEA using two unit cell models.

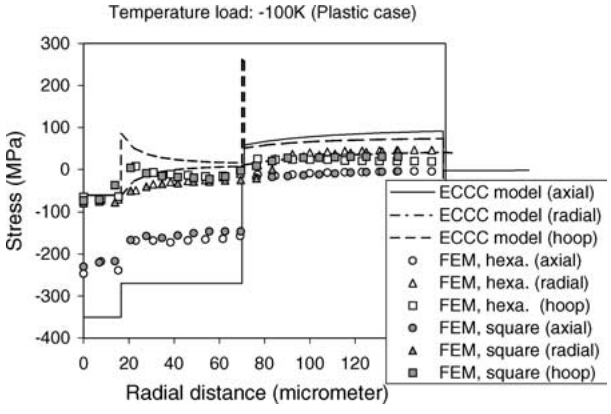

Figure 9 Predicted plastic thermal stress profiles calculated for temperature decrease of 100°C.

Characteristic feature of present model is the combination of incremental mean field micromechanics formulation by Pettermann with the conventional elasticity solution process by Warwick and Clyne. Within this hybrid procedure stress analysis was performed on micro-macro dual scales. This model allowed that the constraint effect of surrounding fibers and plastic flow of matrix could be considered in self-consistent way. The temperature dependence of flow stress could be also included.

Taking copper-SiC (long fiber) system as a reference composite, stress profiles were obtained for mechanical loading (axial stress of 100 MPa) and thermal loading (cooling by 100°C) cases. For comparison and verification, independent finite element analyses were carried out for two different unit cell models.

Excellent agreement between analytical and numerical solutions was found for the mechanical loading. Distribution of the triaxial stress state could be accurately reproduced even in plastic case. In the case of thermal loading, however, such an exact coincidence could not be obtained. While the elastic solution showed similarity to numerical one, plastic solution revealed notable difference, especially for the axial stress component. This was attributed to high thermal stress gradient which could cause numerical errors during mean field homogenization.

Appendix A

In this appendix, a solution process of a three dimensional thermo-elastic problem is given for a cylindrical composite consisting of N concentric material layers [11]. It is assumed that the material properties in each nth layer is transversely isotropic. We consider a general load case that this composite cylinder is subjected to a uniform temperature change ΔT and applied stresses σ_{or} and σ_{oz} in longitudinal and in transverse (i.e., radial) directions, respectively. Whole formulation is described in cylindrical coordinate system.

In the absence of body force, the static equilibrium equations are:

$$\frac{1}{r}\frac{\partial}{\partial r}\left(r\sigma_{\mathrm{rr}}^{(\mathrm{n})}\right)+\frac{1}{r}\frac{\partial\sigma_{\mathrm{r}\theta}^{(\mathrm{n})}}{\partial\theta}+\frac{\partial\sigma_{\mathrm{rz}}^{(\mathrm{n})}}{\partial z}-\frac{\sigma_{\theta\theta}^{(n)}}{r}=0 \quad \text{(A-1a)}$$

$$\frac{1}{r^2}\frac{\partial}{\partial r}\left(r^2\sigma_{\theta\mathrm{r}}^{(\mathrm{n})}\right)+\frac{1}{r}\frac{\partial\sigma_{\theta\theta}^{(\mathrm{n})}}{\partial\theta}+\frac{\partial\sigma_{\theta\mathrm{z}}^{(\mathrm{n})}}{\partial\mathrm{z}}=0 \quad \text{(A-1b)}$$

$$\frac{1}{r}\frac{\partial}{\partial r}\left(r\sigma_{\mathrm{zr}}^{(\mathrm{n})}\right)+\frac{1}{r}\frac{\partial\sigma_{\mathrm{z}\theta}^{(\mathrm{n})}}{\partial\theta}+\frac{\partial\sigma_{\mathrm{zz}}^{(\mathrm{n})}}{\partial\mathrm{z}}=0 \quad \text{(A-1c)}$$

The general thermo-elastic constitutive relations are written as

$$\sigma_{\mathrm{rr}}^{(\mathrm{n})}=C_{11}^{(\mathrm{n})}e_{\mathrm{rr}}^{(\mathrm{n})}+C_{12}^{(\mathrm{n})}e_{\theta\theta}^{(\mathrm{n})}+C_{13}^{(\mathrm{n})}e_{\mathrm{zz}}^{(\mathrm{n})}-\beta_1^{(\mathrm{n})}T_{\mathrm{n}} \quad \text{(A-2a)}$$

$$\sigma_{\theta\theta}^{(\mathrm{n})}=C_{12}^{(\mathrm{n})}e_{\mathrm{rr}}^{(\mathrm{n})}+C_{11}^{(\mathrm{n})}e_{\theta\theta}^{(\mathrm{n})}+C_{13}^{(\mathrm{n})}e_{\mathrm{zz}}^{(\mathrm{n})}-\beta_1^{(\mathrm{n})}T_{\mathrm{n}} \quad \text{(A-2b)}$$

$$\sigma_{\mathrm{zz}}^{(\mathrm{n})}=C_{13}^{(\mathrm{n})}e_{\mathrm{rr}}^{(\mathrm{n})}+C_{13}^{(\mathrm{n})}e_{\theta\theta}^{(\mathrm{n})}+C_{33}^{(\mathrm{n})}e_{\mathrm{zz}}^{(\mathrm{n})}-\beta_3^{(\mathrm{n})}T_{\mathrm{n}} \quad \text{(A-2c)}$$

$$\sigma_{\mathrm{rz}}^{(\mathrm{n})}=2C_{44}^{(\mathrm{n})}e_{\mathrm{rz}}^{(\mathrm{n})} \quad \text{(A-2d)}$$

$$\sigma_{\theta\mathrm{z}}^{(\mathrm{n})}=2C_{44}^{(\mathrm{n})}e_{\theta\mathrm{z}}^{(\mathrm{n})} \quad \text{(A-2e)}$$

$$\sigma_{\mathrm{r}\theta}^{(\mathrm{n})}=\left(C_{11}^{(\mathrm{n})}-C_{12}^{(\mathrm{n})}\right)e_{\mathrm{r}\theta}^{(\mathrm{n})} \quad \text{(A-2f)}$$

where,

$$\beta_1^{(\mathrm{n})}=\left(C_{11}^{(\mathrm{n})}+C_{12}^{(\mathrm{n})}\right)\alpha_{\mathrm{T}}^{(\mathrm{n})}+C_{13}^{(\mathrm{n})}\alpha_{\mathrm{L}}^{(\mathrm{n})} \quad \text{(A-3a)}$$

$$\beta_3^{(\mathrm{n})}=2C_{12}^{(\mathrm{n})}\alpha_{\mathrm{T}}^{(\mathrm{n})}+C_{33}^{(\mathrm{n})}\alpha_{\mathrm{L}}^{(\mathrm{n})} \quad \text{(A-3b)}$$

The linear kinematic relations between infinitesimal strains and displacements are given by

$$e_{\mathrm{rr}}^{(\mathrm{n})}=\frac{\partial u_{\mathrm{r}}^{(\mathrm{n})}}{\partial r} \quad \text{(A-4a)}$$

$$e_{\theta\theta}^{(\mathrm{n})}=\frac{1}{r}\frac{\partial u_{\theta}^{(\mathrm{n})}}{\partial\theta}+\frac{u_{\mathrm{r}}^{(\mathrm{n})}}{r} \quad \text{(A-4b)}$$

$$e_{\mathrm{zz}}^{(\mathrm{n})}=\frac{\partial u_{\mathrm{z}}^{(\mathrm{n})}}{\partial z} \quad \text{(A-4c)}$$

$$e_{\mathrm{rz}}^{(\mathrm{n})}=\frac{1}{2}\left(\frac{\partial u_{\mathrm{z}}^{(\mathrm{n})}}{\partial r}+\frac{\partial u_{\mathrm{r}}^{(\mathrm{n})}}{\partial z}\right) \quad \text{(A-4d)}$$

$$e_{\theta\mathrm{z}}^{(\mathrm{n})}=\frac{1}{2}\left(\frac{\partial u_{\theta}^{(\mathrm{n})}}{\partial z}+\frac{1}{r}\frac{\partial u_{\mathrm{z}}^{(\mathrm{n})}}{\partial\theta}\right) \quad \text{(A-4e)}$$

$$e_{\mathrm{r}\theta}^{(\mathrm{n})}=\frac{1}{2}\left(\frac{1}{r}\frac{\partial u_{\mathrm{r}}^{(\mathrm{n})}}{\partial\theta}+\frac{\partial u_{\theta}^{(\mathrm{n})}}{\partial r}-\frac{u_{\theta}^{(\mathrm{n})}}{r}\right) \quad \text{(A-4f)}$$

The axisymmetry of the model leads to following displacement components

$$u_{\mathrm{r}}^{(\mathrm{n})}=u_{\mathrm{n}}(r) \quad \text{(A-5a)}$$

$$u_{\theta}^{(\mathrm{n})}=0 \quad \text{(A-5b)}$$

$$u_{\mathrm{z}}^{(\mathrm{n})}=w_{\mathrm{n}}(z) \quad \text{(A-5c)}$$

which, by Equation A-4, gives

$$e_{\mathrm{rr}}^{(\mathrm{n})}=\frac{\partial u_{\mathrm{n}}}{\partial r} \quad \text{(A-6a)}$$

$$e_{\theta\theta}^{(\mathrm{n})}=\frac{u_{\mathrm{n}}}{r} \quad \text{(A-6b)}$$

$$e_{zz}^{(n)} = \frac{\partial w_n}{\partial z} \tag{A-6c}$$

$$e_{rz}^{(n)} = e_{\theta z}^{(n)} = e_{r\theta}^{(n)} = 0 \tag{A-6d}$$

Substituting Equation A-6 into Equation A-2, one obtains

$$\sigma_{rr}^{(n)} = C_{11}^{(n)} \frac{\partial u_n}{\partial r} + C_{12}^{(n)} \frac{u_n}{r} + C_{13}^{(n)} \frac{\partial w_n}{\partial z} - \beta_1^{(n)} T_n \tag{A-7a}$$

$$\sigma_{\theta\theta}^{(n)} = C_{12}^{(n)} \frac{\partial u_n}{\partial r} + C_{11}^{(n)} \frac{u_n}{r} + C_{13}^{(n)} \frac{\partial w_n}{\partial z} - \beta_1^{(n)} T_n \tag{A-7b}$$

$$\sigma_{zz}^{(n)} = C_{13}^{(n)} \frac{\partial u_n}{\partial r} + C_{13}^{(n)} \frac{u_n}{r} + C_{33}^{(n)} \frac{\partial w_n}{\partial z} - \beta_3^{(n)} T_n \tag{A-7c}$$

$$\sigma_{rz}^{(n)} = \sigma_{\theta z}^{(n)} = \sigma_{r\theta}^{(n)} = 0 \tag{A-7d}$$

Inserting Equation A-7 into Equation A-1 produces the governing differential equation in terms of displacement components:

$$\frac{d^2 u_n}{dr^2} + \frac{1}{r}\frac{du_n}{dr} - \frac{u_n}{r^2} = l_n \frac{dT_n}{dr} \tag{A-8a}$$

$$\frac{d^2 w_n}{dz^2} = 0 \tag{A-8b}$$

$$l_n = \frac{\beta_1^{(n)}}{C_{11}^{(n)}} \tag{A-8c}$$

Due to the assumption of a uniform temperature field,

$$\frac{dT_n}{dr} = 0 \tag{A-9}$$

Solutions for the differential Equations A-8 take generic forms of

$$u_n(r) = A_n r + \frac{B_n}{r} \tag{A-10a}$$

$$w_n(z) = E_n z + F_n \tag{A-10b}$$

The boundary conditions imposed are

$$\sigma_{rr}^{(n)} = \sigma_{or} \quad \text{at} \quad r = r_N$$

(radial traction on lateral surface) (A-11a)

$$\sum_{n=1}^{N} \int_{r_{n-1}}^{r_n} \sigma_{zz}^{(n)} r \, dr = \int_0^{r_N} \sigma_{oz} r \, dr \quad \text{with}$$

$$r_0 = 0 \text{ (axial traction)} \tag{A-11b}$$

$$u_n = u_{n+1}, \quad w_n = w_{n+1}, \quad \text{at } r = r_n \quad \text{for}$$

$1 \le n \le N-1$ (continuity at material interfaces) (A-11c)

$$\sigma_{rr}^{(n)} = \sigma_{rr}^{(n+1)} \quad \text{at } r = r_n \quad \text{for} \quad 1 \le n \le N-1$$

(force equilibrium at material interfaces) (A-11d)

Without loss of generality we can set

$$F_i = 0 \, (1 \le i \le N) \tag{A-12}$$

From the interface compatibility conditions (A-11c, d)

$$E_i = E (1 \le i \le N) \tag{A-13}$$

Combining Equations A-10 and A-7 gives

$$\sigma_{rr} = C_{11}^{(n)} \left[A_n - \frac{B_n}{r^2} \right] + C_{12}^{(n)} \left[A_n + \frac{B_n}{r^2} \right] + C_{13}^{(n)} E - \beta_1^{(n)} \Delta T \tag{A-14a}$$

$$\sigma_{\theta\theta} = C_{11}^{(n)} \left[A_n + \frac{B_n}{r^2} \right] + C_{12}^{(n)} \left[A_n - \frac{B_n}{r^2} \right] + C_{13}^{(n)} E - \beta_1^{(n)} \Delta T \tag{A-14b}$$

$$\sigma_{zz} = 2 C_{13}^{(n)} A_n + C_{33}^{(n)} E - \beta_3^{(n)} \Delta T \tag{A-14c}$$

Since $u_1(0)$ must remain finite for $T_n = \Delta T$, $B_1 = 0$.

Application of all boundary conditions to Equations A-10 and A-14 yields a system of $2N$ linear simultaneous equations having the form:

$$\boldsymbol{B} = [\boldsymbol{A}]\boldsymbol{C} \tag{A-15}$$

with vectors of $2N$ components

$$\boldsymbol{B} = [b_1 \cdot \cdot b_k \cdot \cdot b_{2N}]^T,$$

$$\boldsymbol{C} = [A_1 \cdot \cdot A_k \cdot \cdot A_N \, B_2 \cdot \cdot B_k \cdot \cdot B_N \, E]^T$$

and a $2N \times 2N$ square matrix

$$[\boldsymbol{A}] = [a_{i,j}].$$

The linear equations system (A-15) is expressed in index notation as

$$\sum_{i=1}^{N} a_{k,i} A_i + \sum_{j=2}^{N} a_{k,(n-1)+j} B_j + a_{k,2N} E = b_k$$

$$\text{for } 1 \le k \le 2N \tag{A-16}$$

The individual groups of the equations which are to be derived from a specific boundary condition are given in the following.

From the continuity conditions (A-11c), we get $N-1$ equations for $1 \le k \le N-1$:

$$A_k r_k - A_{k+1} r_k + \frac{B_k}{r_k} - \frac{B_{k+1}}{r_k} = 0 \tag{A-17a}$$

$$a_{k,k} = r_k \tag{A-17b}$$

$$a_{k,k+1} = -r_k \tag{A-17c}$$

$$a_{k,N+k-1} = \frac{1}{r_k} \tag{A-17d}$$

$$a_{k,N+k} = -\frac{1}{r_k} \tag{A-17e}$$

$$b_k = 0 \tag{A-17f}$$

The equilibrium condition (A-11d) yields $N-1$ equations for $1 \le i \le N-1$ and $k = N+i$

$$A_{\mathrm{i}}\big[C_{11}^{(\mathrm{i})} + C_{12}^{(\mathrm{i})}\big] - A_{\mathrm{i}+1}\big[C_{11}^{(\mathrm{i}+1)} + C_{12}^{(\mathrm{i}+1)}\big] + B_{\mathrm{i}}\left[\frac{C_{12}^{(\mathrm{i})} - C_{11}^{(\mathrm{i})}}{r_{\mathrm{i}}^2}\right] - B_{\mathrm{i}+1}\left[\frac{C_{12}^{(\mathrm{i}+1)} - C_{11}^{(\mathrm{i}+1)}}{r_{\mathrm{i}}^2}\right] + E\big[C_{13}^{(\mathrm{i})} - C_{13}^{(\mathrm{i}+1)}\big] = \Delta T\big(\beta_1^{(\mathrm{i})} - \beta_1^{(\mathrm{i}+1)}\big) \quad \text{(A-18a)}$$

$$a_{\mathrm{k,i}} = \big[C_{11}^{(\mathrm{i})} + C_{12}^{(\mathrm{i})}\big] \quad \text{(A-18b)}$$

$$a_{\mathrm{k,i+1}} = -\big[C_{11}^{(\mathrm{i}+1)} + C_{12}^{(\mathrm{i}+1)}\big] \quad \text{(A-18c)}$$

$$a_{\mathrm{k,N+i-1}} = \left[\frac{C_{12}^{(\mathrm{i})} - C_{11}^{(\mathrm{i})}}{r_{\mathrm{i}}^2}\right] \quad \text{(A-18d)}$$

$$a_{\mathrm{k,N+i}} = -\left[\frac{C_{12}^{(\mathrm{i}+1)} - C_{11}^{(\mathrm{i}+1)}}{r_{\mathrm{i}}^2}\right] \quad \text{(A-18e)}$$

$$a_{\mathrm{k,2N}} = \big[C_{13}^{(\mathrm{i})} - C_{13}^{(\mathrm{i}+1)}\big] \quad \text{(A-18f)}$$

$$b_{\mathrm{k}} = \Delta T\big[\beta_1^{(\mathrm{i})} - \beta_1^{(\mathrm{i}+1)}\big] \quad \text{(A-18g)}$$

The condition of radial traction (A-11a) gives another equation

$$A_{\mathrm{N}}\big[C_{11}^{(\mathrm{N})} + C_{12}^{(\mathrm{N})}\big] + B_{\mathrm{N}}\left[\frac{C_{12}^{(\mathrm{N})} - C_{11}^{(\mathrm{N})}}{r_{\mathrm{N}}^2}\right] + EC_{13}^{(\mathrm{N})} = \sigma_{\mathrm{or}} + \beta_1^{(\mathrm{N})}\Delta T \quad \text{(A-19a)}$$

$$a_{\mathrm{N,N}} = \big[C_{11}^{(\mathrm{N})} + C_{12}^{(\mathrm{N})}\big] \quad \text{(A-19b)}$$

$$a_{\mathrm{N,2N-1}} = \left[\frac{C_{12}^{(\mathrm{N})} - C_{11}^{(\mathrm{N})}}{r_{\mathrm{N}}^2}\right] \quad \text{(A-19c)}$$

$$a_{\mathrm{N,2N}} = C_{13}^{(\mathrm{N})} \quad \text{(A-19d)}$$

$$b_{\mathrm{N}} = \sigma_{\mathrm{or}} + \beta_1^{(\mathrm{N})}\Delta T \quad \text{(A-19e)}$$

The condition of axial traction (A-11b) gives the last simultaneous equation

$$\sum_{\mathrm{i}=1}^{N}\big[2C_{13}^{(\mathrm{i})}A_{\mathrm{i}} + C_{33}^{(\mathrm{i})}E - \beta_3^{(\mathrm{i})}\Delta T\big]\big(r_{\mathrm{i}}^2 - r_{\mathrm{i-1}}^2\big) = \sigma_{\mathrm{oz}}r_{\mathrm{N}}^2 \quad \text{(A-20a)}$$

$$\sigma_{\mathrm{oz}}r_{\mathrm{N}}^2 + \Delta T\sum_{\mathrm{i}=1}^{N}\beta_3^{(\mathrm{i})}\big(r_{\mathrm{i}}^2 - r_{\mathrm{i-1}}^2\big) = \sum_{\mathrm{i}=1}^{N}2A_{\mathrm{i}}C_{13}^{(\mathrm{i})}\big(r_{\mathrm{i}}^2 - r_{\mathrm{i-1}}^2\big) + E\sum_{\mathrm{i}=1}^{N}C_{33}^{(\mathrm{i})}\big(r_{\mathrm{i}}^2 - r_{\mathrm{i-1}}^2\big) \quad \text{(A-20b)}$$

$$a_{\mathrm{2N,i}} = 2C_{13}^{(\mathrm{i})}\big(r_{\mathrm{i}}^2 - r_{\mathrm{i-1}}^2\big), \quad (1 \le i \le N) \quad \text{(A-20c)}$$

$$a_{\mathrm{2N,2N}} = \sum_{\mathrm{i}=1}^{N}C_{33}^{(\mathrm{i})}\big(r_{\mathrm{i}}^2 - r_{\mathrm{i-1}}^2\big) \quad \text{(A-20d)}$$

$$b_{\mathrm{2N}} = \sigma_{\mathrm{oz}}r_{\mathrm{N}}^2 + \Delta T\sum_{\mathrm{i}=1}^{N}\beta_3^{(\mathrm{i})}\big(r_{\mathrm{i}}^2 - r_{\mathrm{i-1}}^2\big) \quad \text{(A-20e)}$$

All other values of $a_{\mathrm{k,j}}$ are set to naught. The unknown coefficients A_{n}, B_{n} and E are then determined by numerical matrix algebra.

Appendix B

In this appendix, essentials of the incremental thermo-elasto-plastic formulation of the Mori-Tanaka mean field theory including related fundamental relationships are shortly summarized.

For fibrous composite materials, the global (macroscopic) thermo-elastic constitutive relation is given by [17]

$$\langle\sigma\rangle = E\langle\varepsilon\rangle + \tau\vartheta, \quad \langle\varepsilon\rangle = C\langle\sigma\rangle + \alpha\vartheta \quad \text{(B-1)}$$

where E and C are the global elastic composite stiffness and compliance matrices, respectively, α stands for the coefficient matrix of linear thermal expansion and $\tau = -E\alpha$ is the global specific thermal stress tensor. The symbol $\langle\ \rangle$ denotes the global volume averaged field quantities.

By analogy, the thermo-elastic constitutive relations for each phase p in micro-scale are written as

$$\langle\sigma\rangle_{\mathrm{tot}}^{(\mathrm{p})} = E^{(\mathrm{p})}\langle\varepsilon\rangle_{\mathrm{tot}}^{(\mathrm{p})} + \tau^{(\mathrm{p})}\vartheta, \quad \text{or}$$
$$\langle\varepsilon\rangle_{\mathrm{tot}}^{(\mathrm{p})} = C^{(\mathrm{p})}\langle\sigma\rangle_{\mathrm{tot}}^{(\mathrm{p})} + \alpha^{(\mathrm{p})}\vartheta \quad \text{(B-2)}$$

where $\langle\ \rangle_{\mathrm{tot}}^{(\mathrm{p})}$ denotes the phase averaged total stress state in the phase p. The superscript p can be either matrix m or fiber i, respectively.

In the case of thermo-elasto-plastic matrix materials, incremental formulation is required for the micromechanical constitutive equations as well as for the mean field homogenization relations. In the following, the computational procedure to estimate the instantaneous state quantities for the thermo-elasto-plastic case are reviewed. The term 'rate' (denoted by d) is used for infinitesimal time derivatives whereas the term 'increment' (denoted by Δ) stands for a finite increment in the context of numerical integration algorithm.

The total averaged strain rates in microstructural phase p can be related to far-field global averaged strain rate by instantaneous mean field strain concentration tensors [16]

$$\mathrm{d}\langle\varepsilon\rangle_{\mathrm{tot}}^{(\mathrm{p})} = \bar{A}_{\mathrm{t}}^{(\mathrm{p})}\, d\langle\varepsilon\rangle_{\mathrm{mech}} + \bar{a}_{\mathrm{t}}^{(\mathrm{p})}\mathrm{d}\bar{\vartheta} \quad \text{(B-3)}$$

where the subscript t denotes instantaneous state and the subscript mech indicates mechanical component. $\bar{A}_{\mathrm{t}}^{(\mathrm{p})}$ is the instantaneous mean field strain concentration tensor and $\bar{a}_{\mathrm{t}}^{(\mathrm{p})}$ stands for the instantaneous mean field thermal strain concentration tensor.

The global instantaneous tangent stiffness E_{t} is formulated as

$$E_{\mathrm{t}} = E^{(\mathrm{i})} + (1-f)\big(E_{\mathrm{t}}^{(\mathrm{m})} - E^{(\mathrm{i})}\big)\,\bar{A}_{\mathrm{t}}^{(\mathrm{m})} \quad \text{(B-4)}$$

and the global instantaneous thermal expansion coefficient α_{t} is given by

$$\alpha_{\mathrm{t}} = (E_{\mathrm{t}})^{-1}\big[\tau^{(\mathrm{i})} + (1-f)\big(\bar{A}_{\mathrm{t}}^{(\mathrm{m})}\big)^{\mathrm{T}}\big(\tau_{\mathrm{t}}^{(\mathrm{m})} - \tau^{(\mathrm{i})}\big)\big] \quad \text{(B-5)}$$

where f is the volume fraction of fibers.

According to Benveniste's formulation, the instantaneous mean field (thermal) strain concentration tensors can be written as [17],

$$\bar{A}_{\mathrm{t}}^{(\mathrm{m})} = \left[(1-f)I + f\left[I + S_{\mathrm{t}}C_{\mathrm{t}}^{(\mathrm{m})}\left(E^{(\mathrm{i})} - E_{\mathrm{t}}^{(\mathrm{m})}\right)\right]^{-1}\right]^{-1} \tag{B-6}$$

$$\bar{a}_{\mathrm{t}}^{(\mathrm{m})} = \left(I - \bar{A}_{\mathrm{t}}^{(\mathrm{m})}\right)\left(E^{(\mathrm{i})} - E_{\mathrm{t}}^{(\mathrm{m})}\right)^{-1}\left(\tau_{\mathrm{t}}^{(\mathrm{m})} - \tau^{(\mathrm{i})}\right) \tag{B-7}$$

in which his original elastic formulation is expressed in terms of the instantaneous state quantities. I denotes the fourth rank identity tensor and S_{t} represents the instantaneous Eshelby tensor. S_{t} is determined using a numerical method developed by Gavazzi and Lagoudas which is based on the Gaussian quadrature [18]. Similar expressions of the instantaneous strain concentration tensors exist for fiber.

We adopt the numerical integration strategy suggested by Pettermann [16]. The core part of this algorithm is the radial return mapping step [19] for stress updating after onset of plastic yield. For the return mapping process, Prandtl-Reuss flow rule is used. The algorithm includes an implicit iteration loop which corrects the Euler backward response of global composite strain to stress relaxation.

Under a combined thermo-mechanical loading, the prescribed global (composite) strain increment $\Delta\varepsilon_{\mathrm{c}}$ is considered to consist of a mechanical contribution $\Delta\varepsilon_{\mathrm{mech}}$ and a thermal contribution $\Delta\varepsilon_{\mathrm{th}} = \alpha_{\mathrm{t}}\Delta\bar{\vartheta}$,

$$\Delta\varepsilon_{\mathrm{c}} = \Delta\varepsilon_{\mathrm{mech}} + \Delta\varepsilon_{\mathrm{th}} \tag{B-8}$$

In the same way, the phase averaged total matrix strain increment can be split into a mechanical and a thermal part as,

$$\Delta\langle\varepsilon\rangle_{\mathrm{tot}}^{(\mathrm{m})} = \Delta\langle\varepsilon\rangle_{\mathrm{mech}}^{(\mathrm{m})} + \alpha^{(\mathrm{m})}\Delta\bar{\vartheta} \tag{B-9}$$

For the prescribed global strain increment $\Delta\varepsilon_{\mathrm{c}}$, the phase averaged mechanical matrix strain increment $\Delta\langle\varepsilon\rangle_{\mathrm{mech}}^{(\mathrm{m})}$ is obtained from Equations B-8 and B-9 as

$$\Delta\langle\varepsilon\rangle_{\mathrm{mech}}^{(\mathrm{m})} = \bar{A}_{\mathrm{t}}^{(\mathrm{m})}\Delta\varepsilon_{\mathrm{c}} + \left(\bar{a}_{\mathrm{t}}^{(\mathrm{m})} - \alpha^{(\mathrm{m})}\right)\Delta\bar{\vartheta} \tag{B-10}$$

First, the mechanical component of the matrix elastic strain increment $\Delta\langle\varepsilon\rangle_{\mathrm{mech}}^{(\mathrm{m})}$ is estimated from Equation (B-10) for current applied global strain increment $\Delta\varepsilon_{\mathrm{c}}$ and temperature $\Delta\bar{\vartheta}$. From the mechanical part of the matrix strain increment $\Delta\langle\varepsilon\rangle_{\mathrm{mech}}^{(\mathrm{m})}$ the total elastic matrix stress increment $\Delta\langle\sigma\rangle_{\mathrm{tot,\,el}}^{(\mathrm{m})}$ is calculated by

$$\Delta\langle\sigma\rangle_{\mathrm{tot,el}}^{(\mathrm{m})} = E_{\mathrm{t}}^{(\mathrm{m})}\Delta\langle\varepsilon\rangle_{\mathrm{mech}}^{(\mathrm{m})}. \tag{B-11}$$

This elastic matrix stress increment $\Delta\langle\sigma\rangle_{\mathrm{tot,el}}^{(\mathrm{m})}$ is superposed onto the instantaneous mechanical matrix stress state obtained in the previous increment step leading to current total stress state in the matrix. Here, $\Delta\langle\sigma\rangle_{\mathrm{tot,el}}^{(\mathrm{m})}$ has the meaning of the elastic predictor in the sense of Euler backward integration. Now, the von Mises yield criterion is checked for matrix. If the yield criterion is fulfilled, return mapping operation is carried out producing a new stress state $\langle\sigma\rangle_{\mathrm{tot}}^{(\mathrm{m})}$ in the matrix. This matrix stress is the updated stress due to plastic relaxation. Next, all state quantities $E_{\mathrm{t}}^{(\mathrm{m})}$, $\bar{A}_{\mathrm{t}}^{(\mathrm{m})}$, $\bar{a}_{\mathrm{t}}^{(\mathrm{m})}$, $\langle\varepsilon\rangle^{(\mathrm{m})}$, $\langle\varepsilon\rangle_{\mathrm{el}}^{(\mathrm{m})}$ and $\langle\varepsilon\rangle_{\mathrm{pl}}^{(\mathrm{m})}$ are updated. To make a correction for the Euler backward response of the composite strain to the updating of matrix strain and of $E_{\mathrm{t}}^{(\mathrm{m})}$ and $\bar{A}_{\mathrm{t}}^{(\mathrm{m})}$, further Euler backward iterations have to be performed in the current incremental step. For the current (for example, nth) iteration step, the Euler backward strain $\Delta\varepsilon_{\mathrm{EB}}$ is obtained as follows

$${}^{\mathrm{n}}\Delta\varepsilon_{\mathrm{EB}} = \left[\bar{A}_{\mathrm{t}}^{(\mathrm{m})}\right]^{-1}\left[\Delta\varepsilon_{\mathrm{mech}}^{(\mathrm{m})} - \left(\bar{a}_{\mathrm{t}}^{(\mathrm{m})} - \alpha^{(\mathrm{m})}\right)\Delta\bar{\vartheta}\right] \tag{B-12}$$

The global sub-increment for the next iteration is obtained as

$${}^{\mathrm{n+1}}\Delta\varepsilon = \Delta\varepsilon_{\mathrm{c}} - \sum_{\mathrm{i}=1}^{n}{}^{\mathrm{n}}\Delta\varepsilon_{\mathrm{EB}} \tag{B-13}$$

This Euler backward implicit iteration loop for the current global strain increment is repeated until ${}^{\mathrm{n+1}}\Delta\varepsilon$ becomes smaller than a given tolerance. Then, the same procedure for the next global strain increment begins. This successively applied global strain sub-increment ${}^{\mathrm{n+1}}\Delta\varepsilon$ can be considered as a feedback corrector for the Euler backward response due to relaxation (return mapping) operation.

For nth iteration, the local fiber stress increment and global stress increment can be obtained as

$${}^{\mathrm{n}}\Delta\langle\sigma\rangle^{(\mathrm{i})} = E^{(\mathrm{i})}\,A_{\mathrm{t}}^{(\mathrm{i})\mathrm{n}}\Delta\varepsilon_{\mathrm{EB}} \tag{B-14}$$

$${}^{\mathrm{n}}\Delta\sigma_{\mathrm{c}} = f\,{}^{\mathrm{n}}\Delta\langle\sigma\rangle^{(\mathrm{i})} + (1-f)\,{}^{\mathrm{n}}E_{\mathrm{t}}^{(\mathrm{m})}\,{}^{\mathrm{n}}\Delta\langle\varepsilon\rangle^{(\mathrm{m})} \tag{B-15}$$

$\langle\sigma\rangle_{\mathrm{tot}}^{(\mathrm{m})}$, $E_{\mathrm{t}}^{(\mathrm{m})}$, $\bar{A}_{\mathrm{t}}^{(\mathrm{m})}$, ${}^{\mathrm{n}}\Delta\sigma_{\mathrm{c}}$ and ${}^{\mathrm{n}}\Delta\sigma^{(\mathrm{i})}$ as well as ${}^{\mathrm{n+1}}\Delta\varepsilon$ and $\Delta\varepsilon_{\mathrm{EB}}$ are updated in every iteration step of each increment, the most recent values of which are taken.

References

1. T. W. CLYNE and P. J. WITHERS, in "An Introduction to Metal Matrix Composites" (Cambridge University Press, Cambridge, 1993).
2. D. WEICHERT, A. HACHEMI and F. SCHWABE, *Arch. Appl. Mech.* **69** (1999) 623.
3. C. GONZALEZ and J. LLORCA, *Acta. Mater.* **49** (2001) 3505.
4. M. H. LIN, W. BUCHGRABER, G. KORB and P. W. KAO, *Scripta. Mater.* **46** (2002) 169.
5. H. J. BÖHM, in "Computer Based Micromechanical Investigations of the Thermomechanical Behavior of Metal Matrix Composites: VDI Berichte Reihe 18 Nr. 101" (VDI Verlag, Düsseldorf, 1991).
6. J. K. KIM and Y. W. MAI, in "Engineered Interfaces in Fiber Reinforced Composites" (Elsevier, Amsterdam, 1998).
7. Y. MIKATA and M. TAYA, *J. Comp. Mater.* **19** (1985) 554.
8. J. D. ESHELBY, *Proc. Roy. Soc. London* A **241** (1957) 376.
9. *Idem.*, *ibid.* A **252** (1959) 561.
10. T. MURA, "Micromechanics of Defects in Solids" (Martinus Nijhoff, Hague, 1982).

11. C. M. WARWICK and T. W. CLYNE, *J. Mater. Sci.* **26** (1991) 3817.
12. J. W. HUTCHINSON and H. M. JENSEN, *Mech. Mater.* **9** (1990) 139.
13. K. TANAKA and T. MORI, *Acta. Metall.* **23** (1973) 571.
14. G. J. DVORAK, in "Plasticity Theories for Fibrous Composite Materials. In Metal Matrix Composites: Mechanisms and Properties" (Academic Press, Boston, 1991).
15. R. M. CHRISTENSEN, *J. Mech. Phys. Solids* **38** (1990) 379.
16. H. E. PETTERMANN, A. F. PLANKENSTEINER, H. J. BÖHM and F. G. RAMMERSTORFER, *Comput. Struc.* **71** (1999) 197.
17. Y. BENVENISTE, *Mech. Mater.* **6** (1987) 147.
18. M. ORTIZ and E. P. POPOV, *Int. J. Num. Mech. Eng.* **21** (1985) 1561.
19. A. C. GAVAZZI and D. C. LAGOUDAS, *Comput. Mech.* **7** (1990) 12.
20. G. J. BUTTERWORTH and C. B. A. *J. Nucl. Mater.* **189** (1992) 237.
21. J. H. YOU, O. POZNANSKY and H. BOLT, *Mater. Sci. Eng. A*, in press.
22. J. R. BROCKENBROUGH, S. SURESH and H. A. WIENECKE, *Acta. Metall. Mater.* **39** (1991) 735.

Received 25 October 2002
and accepted 11 November 2003